NJC

ROYAL SOCIETY OF CHEMISTRY

PAPER

View Article Online
View Journal | View Issue

Cite this: *New J. Chem.*, 2025, **49**, 1745

Synthesis of thiocarbonyl analogues of colourimetric coumarin-based chemosensors: altering the selectivity from Fe to Hg(II) and Cu(II) ions†

Stiaan Schoeman, * Neliswa Mama and Lisa Myburgh

Received 28th November 2024,
Accepted 23rd December 2024

DOI: 10.1039/d4nj05130k

rsc.li/njc

Lawesson's reagent is a thionating compound that can convert a carbonyl group into a thiocarbonyl analogue by replacing oxygen atoms with sulphur. Herein, ester-functionalised coumarin compounds **S1a** and **S2a** were successfully mono-substituted and disubstituted with sulphur atoms using Lawesson's reagent. It was noted that the lactone carbonyl was first substituted, resulting in the mono-substituted analogues **S1b** and **S2b**, followed by the formation of disubstituted derivatives **S1c** and **S2c**. The thionated compounds were separated using preparative TLC with a dichloromethane: petroleum ether mixture as the mobile phase. NMR and FT-IR spectroscopies were utilised to identify and confirm the compounds isolated from the thionation reaction. The thioanalogues were then tested as potential chemosensors for metal ion detection in an acetonitrile solvent system. The results showed unique selectivities, with the unsubstituted derivatives displaying selectivities for Fe^{2+} and Fe^{3+}. In contrast, the mono-substituted and disubstituted derivatives were selective for Hg^{2+} and Cu^{2+}, demonstrating the prospective applications of these compounds as chemosensors for these metal ions.

Introduction

Natural secondary metabolites such as coumarins (2*H*-1-benzopyran-2-ones) are privileged structures due to the oxygen-containing α-pyrone ring fused to a benzene moiety.[1–3] The coumarin moiety is a planar heterocyclic compound that can non-covalently bond to various sites in biological systems.[4] Coumarin derivatives have shown diverse biological activities, such as antimicrobial and anti-cancerous, and can be used as antioxidants, anticoagulants, and anticonvulsants.[5] Furthermore, coumarins have a highly flexible moiety that is easily modified, leading to coumarins being widely studied.[6,7] The ability of coumarins to be easily modified and form non-covalent bonds and their photophysical properties have led them to be used as the core of numerous chemosensors.[8–10]

Chemosensors are sensors in the field of host–guest chemistry. Chemosensors are compounds that convert an interactive response into a measurable signal that can be used to identify or determine the concentration of an analyte. Chemosensors have rapidly expanded over the last few decades due to their advantages over traditional detection methods. Conventional analytical techniques include atomic emission spectroscopy (AES), atomic absorption spectroscopy (AAS), electrochemical techniques, surface plasmon resonance, inductively coupled plasma mass spectrometry (ICP-MS) and X-ray spectroscopic methods. These traditional analytical techniques have many advantages; however, they suffer similar disadvantages, including weak sensitivity and selectivity, poor signal-to-noise ratios, signal drifts, high costs associated with these techniques, and specialised sample preparation and technicians required for operations.[11,12] Chemosensors have thus been employed due to their simplicity, fast response time and reliable detection while still having high sensitivity and selectivity.[12]

Mercury is a heavy metal commonly found in the +1 and +2 oxidation states.[13–15] This metal ion can be exposed to the environment through volcanic and geothermal springs and geological deposits.[16–18] Mercury cations are highly toxic and can cause various health problems in multiple organisms. The high affinity of mercury for sulphur atoms is attributed to the soft base and soft acid nature of the sulphur and mercury atoms, causing a covalent bond to form.[19,20] The soft acid properties of mercury are associated with its large size, high polarisability, and low electronegativity.[21] The affinity of mercury(II) ions for sulphur atoms was used to design a coumarin-based chemosensor that is selective for mercury cations. A carbonyl oxygen can be converted to a thiocarbonyl functional group using a thionating reagent.[22]

Department of Chemistry, Nelson Mandela University, Gqeberha, Eastern Cape, South Africa. E-mail: Stiaan.schoeman@mandela.ac.za, Neliswa.mama@mandela.ac.za, s219004889@mandela.ac.za

† Electronic supplementary information (ESI) available. See DOI: https://doi.org/10.1039/d4nj05130k

Lawesson's reagent is the most popular thionating reagent, and it is synthesised using phosphorus pentasulphide and anisole.[23]

Results and discussion

Synthesis of thionated chemosensors

Coumarin derivatives were synthesised *via* the Knoevenagel condensation reaction, as shown by the first reaction step in Scheme 1.[24,25] The two coumarin derivatives **S1a** and **S2a** were then reacted with Lawesson's reagent to convert the carbonyl groups from the lactone ring and ester moiety to the corresponding sulphur analogues.

The reaction yielded two compounds in which the major product (derivatives **S1b** and **S2**b) was identified as the mono-substituted coumarin analogue in which only the carbonyl from the lactone rings was thionated. As shown in Fig. 1, the lactone carbonyl carbon (▲) of **S2a** shifted from 156 ppm (Fig. 1(b)) to 191 ppm in the thiocarbonyl analogue **S2b** (Fig. 1(a)). The ethyl carbon (★) from the ester unit remained at 62 ppm, indicating that the ester carbonyl (●) had not been thionated. A second compound was isolated as a minor product and was identified as the disubstituted (derivatives **S1c** and **S2c**) thiocarbonyl analogues. As with the mono-substituted analogues, in Fig. 1(c) the lactone carbonyl carbon (▲) shifted from 156 to 191 ppm. However, the ester carbonyl carbon (●) shifted from 163 ppm (Fig. 1(b)) to 211 ppm (Fig. 1(c)) which indicated that both carbonyls were thionated. In addition, the ethyl carbon (★) from the ester moiety shifted from 62 to 69 ppm due to the thionation. (^{1}H and ^{13}C NMR overlay of all compounds can be found in ESI† Fig. S1–S25).

The shift in the carbon-13 peaks caused by the thionation was observed to be relatively constant between the two groups (**S1** and **S2**), as shown in Table S1 in the ESI.†

FT-IR studies were also performed on the synthesised compounds, as seen in Fig. 2 and in the ESI† (Fig. S7, S10, S13, S17, S21, and S25). In Fig. 2(a) the two carbonyl carbon peaks, 1735 and 1701 cm^{-1}, for **S2a** are clearly visible (indicated by ● and ▲) as expected. However, in Fig. 2(b) after the first thionation, the first peak (●) shifted to 1728 cm^{-1} and the second carbonyl peak (▲) has disappeared (indicated by the blue dashed box), thus indicating the replacement of the carbonyl oxygen by sulphur to form the corresponding thiocarbonyls **S1b** and **S2b**. Moreover, in Fig. 2(c) both carbonyl functional groups have disappeared, indicating that both these carbonyl functional groups have been thionated, confirming the formation of the disubstituted compounds **S1c** and **S2c**.

The thionation reaction was monitored by thin-layer chromatography (TLC) and developed using a 60 : 40 mixture of dichloromethane and petroleum ether. Aliquots were taken hourly and are shown in ESI† Fig. S26. After the first hour, the mono-substituted thio-coumarin derivative (**S1b**) was observed visually (orange spot in (a)) and under the UV light (black spot in (b)). Subsequently, after two hours, trace amounts of the disubstituted thiocoumarin derivative (**S1c**) were only visible under UV light indicated by the red dotted line in (b). The concentration of **S1c** increased and after four hours, **S1c** was visible under ambient light indicated by the blue dotted line in (a). The TLC plates showed that the disubstituted compounds formed *via* sequential substitution.

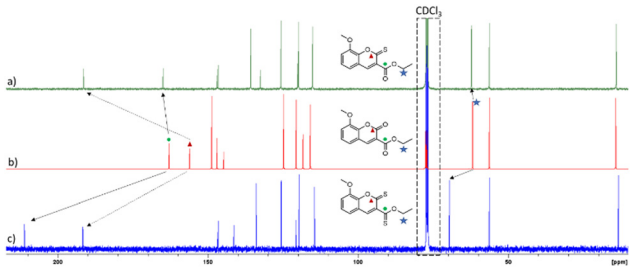

Fig. 1 ^{13}C NMR spectral overlay of (a) **S2b,** (b) **S2a,** and (c) **S2c**.

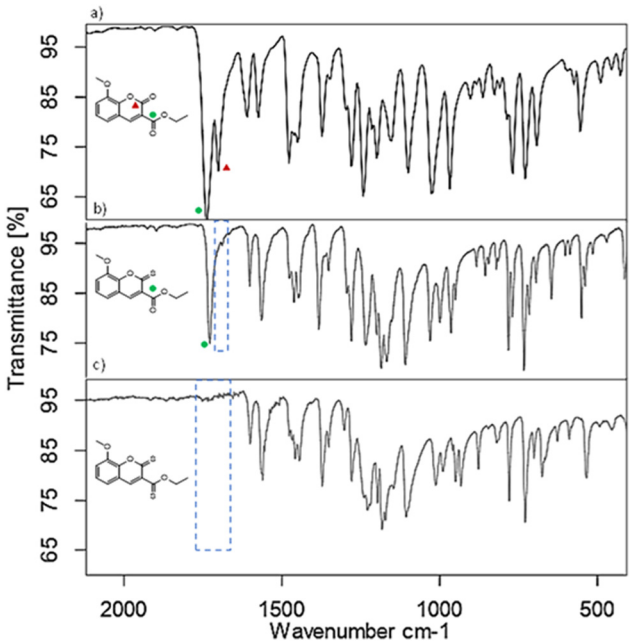

Fig. 2 FT-IR spectra of compounds (a) **S2a**, (b) **S2b**, and (c) **S2c**.

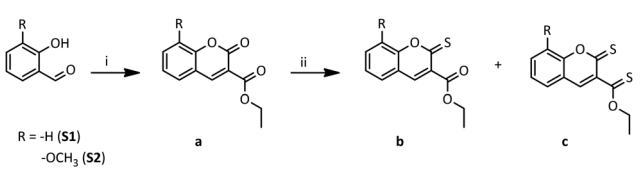

Scheme 1 General synthetic pathway to obtain the thiocoumarin derivatives. (i) Diethyl malonate, piperidine, ethanol GAA, 2 h reflux. (ii) Lawesson's reagent, toluene, 8 h reflux, N_2.

UV-Visible spectroscopy analysis

The application of these thionated compounds as chemosensors for detecting metal ions was evaluated using UV-vis spectral analysis in acetonitrile at room temperature.

Metal ion screening

The metal ions were screened by adding a solution of various metal nitrate salts to a quartz cuvette containing these compounds in acetonitrile and measuring the absorbance. A

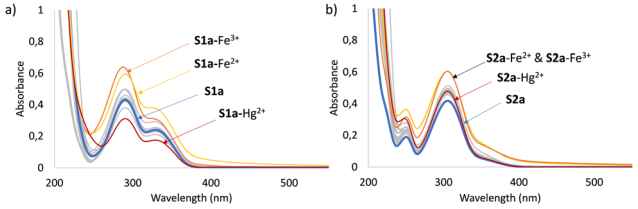

Fig. 3 Metal screening absorption studies of chemosensors (a) **S1a** and (b) **S2a**. The chemosensors are indicated in blue, Fe^{2+} in yellow, Fe^{3+} in orange, Hg^{2+} in red, and all other metal complexes in grey.

change in the absorbance was attributed to the complexation between the chemosensor and the metal analyte.

Compounds **S1a** and **S2b** (shown in blue in Fig. 3) displayed a strong absorbance band between 250 nm and 340 nm, which could be attributed to the π–π* transition in the coumarin moiety.[10] The addition of metal ions, as seen in Fig. 3, caused an increase in the absorbance of these compounds. In the presence of both Fe^{2+} and Fe^{3+} ions, the absorbance was increased substantially compared to the spectra of **S1a** and **S2a** alone (shown in blue). Notably in Fig. 3(a), the **S1a**–Hg^{2+} complex had lower absorbance compared to **S1a**, whereas **S2a**–Hg^{2+} had a slight increase in absorbance compared to **S2a** alone (Fig. 3(b)).

The substitution on the thiolactone group resulted in a broad new band between 310 nm and 460 nm, attributed to the introduction of the sulfurs' nonbonding electron pair to a pi antibonding orbital (n–π*) transition.[26] The metal screening for the mono-substituted coumarin analogue is shown in Fig. 4. The most notable changes observed between the chemosensors **S1a** and **S2a** and the thionated analogues **S1b** and **S2b** were the absorbance spectra of the Hg^{2+} complexes, which in both produced a strong band at 390 nm for **S1b** (Fig. 4(a)) and 395 nm for **S2b** (Fig. 4(b)). Additionally, the Fe^{2+} and Fe^{3+} complexes for **S1b** and **S2b** were less pronounced, indicating that the sulphur atom in the lactone ring affected the interactions.

With the addition of the second sulphur atom in the disubstituted analogue, the π–π* transition band between 250 nm and 320 nm broadened and decreased due to the additional n–π* transition of the second thiocarbonyl group. In the screening analysis, Fe^{2+} and Fe^{3+} complexes persisted with an increase in absorbance, as seen in Fig. 5. Surprisingly, both Hg^{2+} and Cu^{2+} complexes significantly decreased the absorbance around the 400 nm band. As seen in the inset in Fig. 5(b), this decrease in the absorbances is accompanied by a change in colour from the yellow solution to a clear solution in the

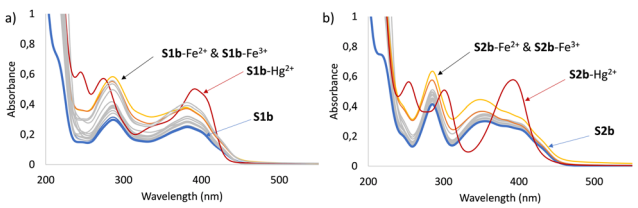

Fig. 4 Metal screening absorption studies of chemosensors (a) **S1b** and (b) **S2b**. The chemosensors are indicated in blue, Fe^{2+} in yellow, Fe^{3+} in orange, Hg^{2+} in red, and all other metal complexes in grey.

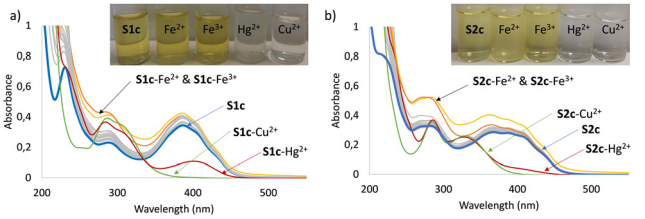

Fig. 5 Metal screening absorption studies of chemosensors (a) **S1c** and (b) **S2c**. The chemosensors are indicated in blue, Fe^{2+} in yellow, Fe^{3+} in orange, Cu^{2+} in green, Hg^{2+} in red, and all other metal complexes are displayed in grey. Inset (a): Photograph of solutions containing, from the left, **S1c**, **S1c**–Fe^{2+}, **S1c**–Fe^{3+}, **S1c**–Hg^{2+}, and **S1c**–Cu^{2+}. Inset (b): Photograph of solutions containing, from the left, **S2c**, **S2c**–Fe^{2+}, **S2c**–Fe^{3+}, **S2c**–Hg^{2+}, and **S2c**–Cu^{2+}.

presence of Hg^{2+} and Cu^{2+}. As discussed in the Introduction section, the interactions between sulphur and mercury were attributed to soft–soft interactions. Copper is a borderline Lewis acid and therefore can also form soft–soft interactions.[27,28] Thio-copper(II) complexes have been observed in the literature,[29,30] although thio-copper(I) complexes are more common.[31–33]

Selectivity studies

Selectivity studies were conducted to determine the preference of a chemosensor towards a specific analyte in the presence of a competing analyte. These studies were conducted by adding a solution of the chemosensor to the solution containing two equimolar analytes; the change in absorbance indicates the preferred complex. When the selectivity profile of **S1a** was evaluated, it was observed that **S1a** was not selective for Fe^{3+} (Fig. S27, ESI†), which gave the strongest response during the screening process (Fig. 3(a)). Poor selectivity was observed when the mono-substituted chemosensors **S1b** and **S2b** were analysed towards Hg^{2+} in the presence of all metal cations (Fig. S28, ESI†). However, the disubstituted analogues (**S1c** and **S2c**) showed remarkable selectivity towards both Hg^{2+} and Cu^{2+} analytes in the presence of other competing metal ions. Furthermore, Cu^{2+} was preferred over Hg^{2+}, as indicated in Fig. 6 and Fig. S29 (ESI†). When both Cu^{2+} and Hg^{2+} were present in the solution, both **S1c** and **S2c** preferred Cu^{2+} as the absorbance intensity at 390 nm more closely

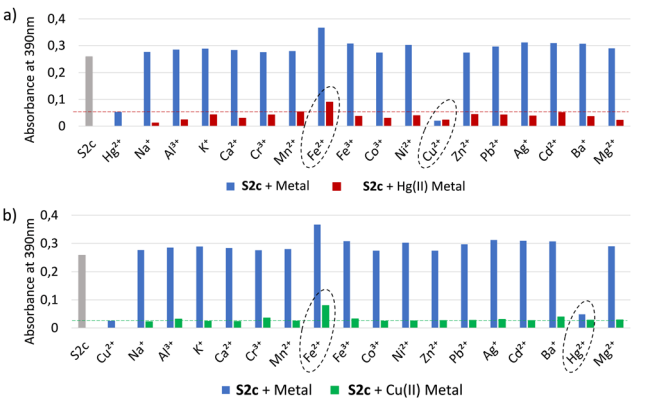

Fig. 6 Selectivity studies for **S2c** towards (a) Hg^{2+} and (b) Cu^{2+}.

resembles that of Cu^{2+}. As mentioned earlier, it was suspected that Hg^{2+} would be the preferred analyte due to the soft–soft Lewis acid and base interactions; however, it was observed that the borderline Lewis acid, Cu^{2+}, was the preferred analyte. Many variables can affect the hardness of Lewis acids and bases, such as the fractional charge of the atoms,[34] solvents used,[35] and the interaction between reactants;[34] therefore, the hardness value of Hg^{2+}, Cu^{2+} and sulphur (from the sensor) can fluctuate and affect the complexes that form.

It was also observed that Fe^{2+} (a borderline Lewis acid) slightly interfered with the sensing ability of both **S1c** and **S2c** for both Hg^{2+} and Cu^{2+}.

Titration studies

UV-Vis titration studies were conducted on all relevant chemosensors by gradually increasing the amount of the selected metal ion to determine the binding stoichiometry, the limit of quantification (LOQ), the limit of detection (LOD), and to construct the calibration curve. The studies were conducted in acetonitrile at room temperature. Titration curves for the mono-substituted analogue can be found in the ESI† (Fig. S30); a linear increase in absorbance was observed for both **S1b** and **S2b** with the addition of Hg^{2+}, and the saturation point (SP) was reached after the addition of 20 μM and 60 μM, respectively. Both Hg^{2+} and Cu^{2+} were used for titrations for **S1c** (Fig. S31, ESI†) and **S2c** (Fig. 7) and a linear decrease in absorbance was observed for all titration studies of **S1c** and **S2c**. Interestingly, **S1c** displayed a decrease in absorbance at 390 nm and an increase in absorbance at 280 nm, creating an isosbestic point at 335 nm. This was also observed with **S2c**, where the decrease in absorbance was also at 390 nm, and the increase in the absorbance band was shifted to 330 nm, resulting in the isosbestic point occurring at 340 nm.

Using the titration data at 390 nm, calibration curves were constructed for these compounds (Fig. S32, S33, ESI† and Fig. 8). The obtained results were used not only to construct the calibration curve, which could be used to calculate the concentration of an unknown sample but also to determine the LOD and the LOQ. The LOD is the lowest concentration of the analyte that a chemosensor can reliably detect, whereas the LOQ is the lowest concentration that can be accurately measured. Table 1 illustrates the LOD, LOQ and SP of all the chemosensors in the presence of their selected metal cations. It was observed that the disubstituted compounds (**S1c** and **S2c**) generally had a broader detection range

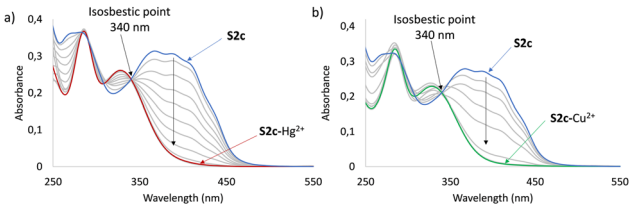

Fig. 7 Titration studies of **S2c** with increasing amounts of (a) Hg^{2+} and (b) Cu^{2+}. Both graphs show an isosbestic point at 340 nm.

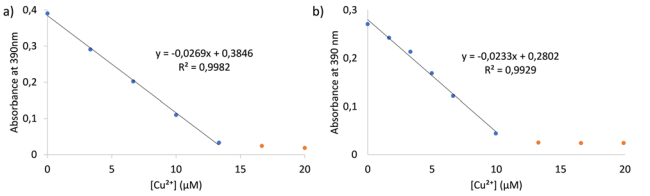

Fig. 8 Calibration curve for (a) **S1c** and (b) **S2c** with the increase of Cu^{2+}.

Table 1 Summary of the LOD, LOQ and SP for all relevant chemosensors

	S1b	S1c		S2b	S2c	
	$[Hg^{2+}]$ (μM)	$[Hg^{2+}]$ (μM)	$[Cu^{2+}]$ (μM)	$[Hg^{2+}]$ (μM)	$[Hg^{2+}]$ (μM)	$[Cu^{2+}]$ (μM)
LOD	3.78	4.56	0.85	3.75	1.94	1.12
LOQ	11.47	13.83	2.57	11.37	5.89	3.40
SP	20.00	46.67	13.33	20.00	26.51	9.96

compared to the mono-substituted chemosensors **S1b** and **S2b**. Furthermore, **S1c** and **S2c** displayed a lower LOD and LOQ towards Cu^{2+} than those of Hg^{2+}.

Benesi–Hildebrand plot and Job's plot and bonding predictions

The absorbance, at 390 nm, from the titration curves was used to construct the Benesi–Hildebrand plots for all relevant chemosensors (Fig. S34, S35, ESI† and Fig. 9). The binding constants were calculated and are shown in Table 2. The highest binding constants were observed for **S1c**–Cu^{2+} and **S2c**–Cu^{2+} with binding constants of 32 784.59 M^{-1} and 16 319.59 M^{-1}, respectively, thus further confirming the selectivity towards Cu^{2+}. The plots also indicated that all complexes formed a 1 : 1 binding ratio due to the linearity of the trend line; this was further confirmed by performing Job's plot experiment, which showed a 1 : 1 binding ratio during complexation (Fig. S36, ESI†).

Molecular modelling and carbon-13 studies

Spartan software was utilised to visualise the binding of the various complexes formed in the presence of Hg^{2+} and Cu^{2+}. We have previously shown in our group a metal analyte complex between the lactone carbonyl and the ester carbonyl,[10] as illustrated in Scheme 2 using the thio analogue. This was again confirmed using carbon-13 NMR shown in Fig. 10.

DFT calculations of the free coumarin derivatives showed that the coumarin moiety exists in a planar geometry with the ester side chain at position 3 freely rotating out of the plane;

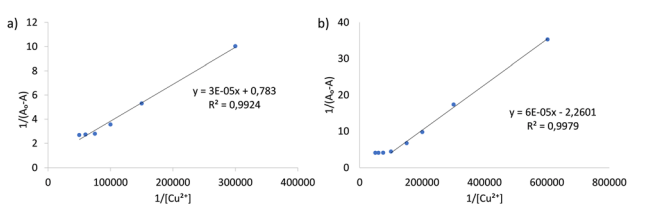

Fig. 9 The Benesi–Hildebrand plot for (a) **S1c** and (b) **S2c** in the presence of Cu^{2+}.

Table 2 Summary of the binding constants (BC) and binding ratios (BR) of all relevant chemosensors

	S1b	S1c		S2b	S2c	
	$[Hg^{2+}]$ (μM^{-1})	$[Hg^{2+}]$ (μM^{-1})	$[Cu^{2+}]$ (μM^{-1})	$[Hg^{2+}]$ (μM^{-1})	$[Hg^{2+}]$ (μM^{-1})	$[Cu^{2+}]$ (μM^{-1})
BC	5065.81	8412.23	32 784.59	14 043.72	5250.83	16 319.59
BR	1 : 1	1 : 1	1 : 1	1 : 1	1 : 1	1 : 1

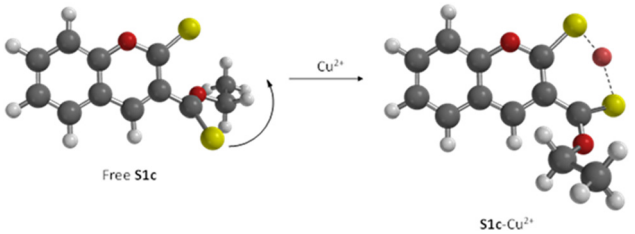

Scheme 2 Computational calculations illustrating the complexation between the two thiocarbonyl groups of **S1c** and Cu^{2+}.

however, the carbonyl ester was observed to be pointing away from the lactone carbonyl due to the electrostatic repulsion of oxygen and sulphur atoms.

During complexation, the thioester group rotates towards the thiolactone group, overcoming the electrostatic repulsion due to the positively charged metal ions, to form the **S1c**–Cu^{2+} complex, thereby yielding a stabilising 6-membered ring structure at the binding site between the two thiocarbonyl groups.

As mentioned, carbon-13 NMR analysis was performed to confirm the binding site observed in Scheme 2. To achieve this, the ^{13}C NMR spectrum of **S1c** was obtained and compared to the spectrum of the **S1c**–Cu^{2+} complex (Fig. 10(a)). The two thiocarbonyl carbon peaks observed at 192 ppm and 210 ppm in **S1c** (Fig. 10(b)) completely disappeared in the presence of Cu^{2+} ions, illustrating the involvement of both sulphur atom interactions during complexation.

Reversibility studies

Reversibility studies were conducted on the Hg^{2+} and Cu^{2+} complexes for chemosensors **S1c** (Fig. S37, ESI†) and **S2c** (Fig. 11) using EDTA as the chelating agent. Upon the addition

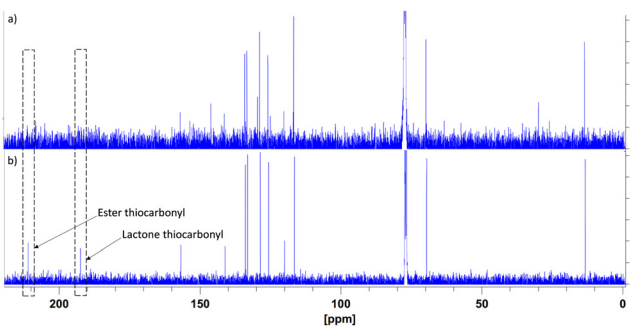

Fig. 10 ^{13}C NMR spectra of (a) **S1c**–Cu^{2+} and (b) **S1c**.

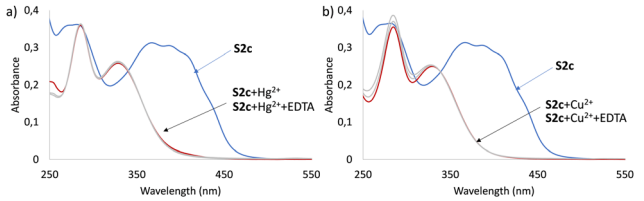

Fig. 11 Reversibility studies of **S2c** with (a) Hg^{2+} and (b) Cu^{2+} in the presence of EDTA.

of excess EDTA to the complexes, there were no significant changes noted in the absorbances, indicating that both complexes (Fig. 11(a) and (b)) were not reversible.

Real-life application studies

Real-world water samples are complex matrices of different substances that could interfere with the chemosensors' ability to detect the preferred analyte. Therefore, mono-substituted **S2b** and the disubstituted **S2c** chemosensor abilities were further tested using lake water as the complex real-world water samples, collected from the North End Lake, Gqeberha, Eastern Cape, South Africa. Pharmaceutical companies, factories and the iconic Nelson Mandela Bay Stadium surround the North End Lake, which could contribute to the contamination/pollution.

However, when the collected samples from the lake were tested for target metal ions, the amount present was too low to be detected using our chemosensors. Hence, the samples were spiked with known concentrations of Hg^{2+} and Cu^{2+}, as shown in Fig. 12 and 13.

The mono-substituted thiocoumarin derivative **S2b** showed a change in its colourimetric properties from yellow to clear in the presence of an increasing concentration of Hg^{2+} shown in Fig. 12. At a low mercury concentration, 33.3 μM, the solution's colour slightly decreased. A notable decrease was observed in the presence of 66.7 μM Hg^{2+}, which continued with higher concentrations; however, a clear solution was not observed.

The disubstituted thiocoumarin derivative **S2c** was also tested for its real-world practicality in detecting dissolved Hg^{2+} using the spiked North End Lake water. **S2c** showed a gradual colourimetric change from yellow to clear with the increase of Hg^{2+} as seen in Fig. 13(a). A notable change is observed in the presence of 33.3 μM Hg^{2+}, which gradually lightens in colour till a clear solution is observed in the presence of 166 μM Hg^{2+}. **S2c** was also tested in the presence of Cu^{2+}, Fig. 12 and 13(b). A much lower

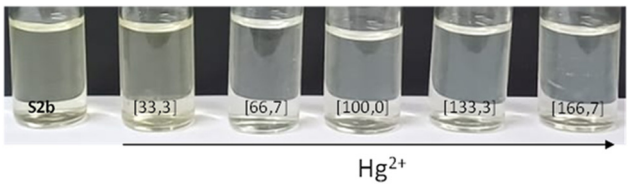

Fig. 12 Real-world application study of the mono-substituted **S2b** (166.7 μM) chemosensor using the North End Lake water samples spiked with Hg^{2+} (μM).

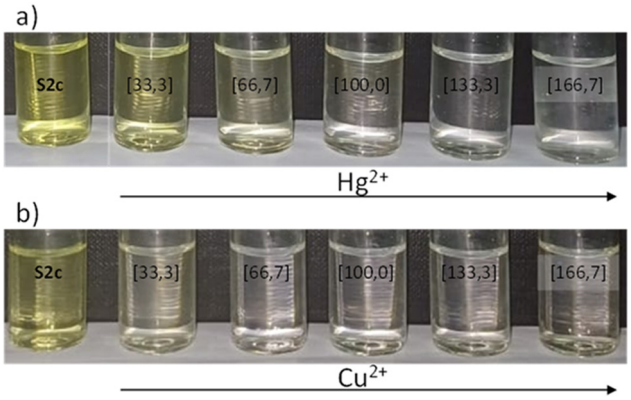

Fig. 13 Application study of the disubstituted **S2c** (166.7 μM) chemosensor using the North End Lake water samples (a) spiked with Hg^{2+} (μM) and (b) spiked with Cu^{2+} (μM).

concentration of 100.0 μM was required to produce a clear solution; this indicated and reiterated that the disubstituted thiocoumarin derivative was much more sensitive towards Cu^{2+} identification.

Experimental

All the chemicals used for synthesis and analysis were purchased from Sigma Merck and used without further purification. The reactions were monitored using thin-layer chromatography (TLC) and nuclear magnetic resonance (NMR) spectroscopy. The TLC plates were pre-coated silica gel 60 F254 aluminium sheets with 0.063–0.2 mm/70–230 mesh plates. A 60 : 40% dichloromethane-PET ether solution was used unless otherwise stated. The plates were monitored under UV light to observe the formation of synthesised compounds. The formation of the compounds was confirmed using NMR spectra using a Bruker Advance DPX 400 (400 MHz) spectrometer. The samples were prepared in $CDCl_3$ or CD_3CN with tetramethyl silane (TMS) as the internal reference. The chemical shift of the NMR is recorded in parts per million (ppm). The FT-IR spectra were obtained using a Bruker TENSOR 27 spectrometer. UV-Vis analysis was conducted at room temperature using a Shimadzu UV-3100 spectrophotometer and the UV Probe v2.42 software. Computational studies were carried out using Spartan Student v9.03, 2023 software. Elemental analysis was outsourced and performed by the University of KwaZulu-Natal.

Synthetic procedures

Scheme 1 outlines the general synthetic route taken to synthesise the desired thionated analogues of **S1a** and **S2a** and confirmed using NMR, FT-IR and elemental analysis (for ^{1}H NMR, ^{13}C NMR, and FT-IR of all the products, see ESI† Fig. S.1–S.25).

Synthesis of coumarin derivatives

Ethyl 2-oxo-2*H*-chromene-3-carboxylate, S1a. Diethyl malonate (8.01 g, 50.00 mmol) was added to salicylaldehyde (10.91 g, 50.00 mmol), 1 mL of piperidine, and five drops of glacial acetic acid in 25 mL EtOH. The mixture was refluxed for two hours, after which the mixture was placed in an ice bath, and the resulting precipitate was filtered and dried to afford the ethyl 2-oxo-2*H*-chromene-3-carboxylate derivative, **S1a**, as a white solid. Yield: 47%. ^{1}H NMR: ($CDCl_3$) δ_H: 1.42–1.45 (t, 3H), 4.41–4.47 (q, 2H), 7.34–7.39 (m, 2H), 7.63–7.69 (m, 2H), 8.54 (s, 1H). ^{13}C NMR ($CDCl_3$) δ_C: 14.24, 62.00, 116.82, 117.92, 118.42, 124.84, 129.49, 134.32, 148.57, 155.21, 156.71, 163.10. IR ν_{max} (cm^{-1}): 3065–2914 (C–H), 1761 (C═O).[24]

Ethyl 8-methoxy-2-oxo-2*H*-chromene-3-carboxylate, S2a. Diethyl malonate (6.30 g, 39.33 mmol) was added to *o*-vanillin (5.00 g, 32.82 mmol), 1 mL piperidine, and five drops of glacial acetic acid in 25 mL EtOH. The mixture was refluxed for two hours, after which the mixture was put onto ice, and the resulting precipitate was filtered and dried to afford the ethyl 2-oxo-2*H*-chromene-3-carboxylate derivative, **S2a**, as a white solid. Yield: 95%. ^{1}H NMR: ($CDCl_3$) δ_H: 1.33–1.37 (t, 3H), 3.91 (s, 3H), 4.32–4.37 (q, 2H), 7.12–7.22 (m, 3H), 8.43 (s, 1H). ^{13}C NMR ($CDCl_3$) δ_C: 14.18, 56.27, 61.84, 115.86, 118.29, 118.35, 120.60, 124.74, 144.70, 146.94, 148.74, 156.12, 162.92. IR ν_{max} (cm^{-1}): 3040–2854 (C–H), 1735 (C═O), 1701 (C═O).[24]

Synthesis of Lawesson's reagent

Anisole (270 g, 2.50 mol) was added to phosphorus sulfide (111.0 g, 0.25 mol). The mixture was refluxed, and after two hours, the product precipitated. When the reaction was complete, the mixture was cooled to room temperature. The resulting precipitate was filtered and washed with anhydrous ether and anhydrous chloroform (alcohol-free).[36] 2,4-Bis(4-methoxyphenyl)-1,3,2,4-dithiadiphosphetane-2,4-disulfide (Lawesson's reagent) was isolated as a pale yellow solid. Yield: 80%.

Synthesis of thiocoumarin analogues

General thionation reaction

The respective coumarin derivative (8.06 mmol) and Lawesson's reagent (16.12 mmol) were combined and dissolved in 25 mL of dry toluene. The mixture was refluxed for eight hours under an N_2 atmosphere, after which the mixture was poured into water and extracted with ethyl acetate. The ethyl acetate extracts were washed with brine water and distilled water. The ethyl acetate was dried with anhydrous $NaSO_4$, and the solvent was removed under reduced pressure. Two compounds were isolated using prep plates (60 : 40, DCM : PET ether).[37]

Major products

Ethyl 2-thioxo-2*H*-chromene-3-carboxylate, S1b. S1b was isolated as a dark orange solid. ^{1}H NMR: ($CDCl_3$) δ_H: 1.42–1.45 (t, 3H), 4.41–4.47 (q, 2H), 7.36–7.39 (t, 1H), 7.48–7.61 (d–d, 2H), 7.66–7.70 (t, 1H), 7.88 (s, 1H). ^{13}C NMR ($CDCl_3$) δ_C: 14.06, 62.28, 116.58, 119.44, 125.73, 128.76, 132.31, 133.78, 135.62, 157.01, 164.89, 192.16. IR ν_{max} (cm^{-1}): 3055–2930 (C–H), 1718 (C═O). $C_{12}H_{10}O_3S$: 58.37% C, 4.48% H, 11.97% S.

Ethyl 8-methoxy-2-thioxo-2*H*-chromene-3-carboxylate, S2b. S2b was isolated as a light orange solid. ^{1}H NMR: ($CDCl_3$) δ_H: 1.41–1.45 (t, 3H), 4.01 (s, 3H), 4.41–4.44 (q, 2H), 7.14–7.19

(m, 2H), 7.29–7.31 (m, 1H), 7.85 (s, 1H). ^{13}C NMR ($CDCl_3$) δ_C: 14.06, 56.32, 62.24, 115.13, 119.78, 120.13, 125.69, 132.54, 135.72, 146.61, 146.98, 164.94, 191.38. IR ν_{max} (cm^{-1}): 3022–2852 (C–H), 1728 (C═O). $C_{13}H_{12}O_4S$: 59.48% C, 4.47% H, 11.28% S.

Minor products

***O*-Ethyl 2-thioxo-2*H*-chromene-3-carbothioate, S1c. S1c** was isolated as a light orange solid. ^{1}H NMR: ($CDCl_3$) δ_H: 1.51–1.55 (t, 3H), 4.71–4.77 (q, 2H), 7.34–7.38 (t, 1H), 7.48–7.60 (d–d, 2H), 7.62–7.66 (t, 1H), 7.77 (s, 1H). ^{13}C NMR ($CDCl_3$) δ_C: 13.33, 69.56, 116.48, 119.97, 119.97, 125.64, 128.56, 133.06, 133.87, 141.11, 156.11, 192.40, 210.96. IR ν_{max} (cm^{-1}): 3050–2840 (C–H). $C_{12}H_{10}O_2S_2$: 55.30% C, 4.21% H, 24.62% S.

***O*-Ethyl 8-methoxy-2-thioxo-2*H*-chromene-3-carbothioate, S2c. S2c** was isolated as a brown solid. ^{1}H NMR: ($CDCl_3$) δ_H: 1.51–1.54 (t, 3H), 4.01 (s, 3H), 4.71–4.76 (q, 2H), 7.13–7.16 (m, 2H), 7.28–7.29 (m, 1H), 7.74 (s, 1H). ^{13}C NMR ($CDCl_3$) δ_C: 13.33, 25.32, 69.54, 114.53, 119.67, 120.69, 125.59, 133.97, 141.33, 146.61, 146.74, 191.63, 211.05. IR ν_{max} (cm^{-1}): 3015–2845 (C–H). $C_{13}H_{12}O_3S_2$: 55.81% C, 4.40% H, 23.84% S.

Materials and methods

Spectroscopic measurements

Various metal stock solutions of 0.01 M were prepared by dissolving the appropriate nitrate salts in deionised water. The stock solution of the coumarin-based chemosensors was prepared in a solvent system containing a 50 : 50 ratio of DCM and acetonitrile to achieve a concentration of 0.01 M. The metal screening investigation was conducted by adding 33.33 μM aliquots of the chosen metal ions and 33.33 μM of the coumarin-based chemosensor to acetonitrile in a 3 mL quartz cuvette. The competition studies were investigated in an acetonitrile solvent system. To the quartz cuvette, 33.33 μM of the selective metal cation, 33.33 μM of the competing metal cation and 33.33 μM of the chemosensor were added to acetonitrile. The spectral response of the chemosensor was investigated using UV-analysis between absorbances of 200 and 600 nm. This study was carried out at room temperature. Titration studies were performed by increasing the concentrations of the selected metal cation in a solution of acetonitrile and the chemosensor (a constant concentration of 33.33 μM), and the spectral change was analysed.

These metal cations include Na^+, Mg^{2+}, Al^{3+}, K^+, Ca^{2+}, Cr^{3+}, Mn^{2+}, Fe^{2+}, Fe^{3+}, Co^{3+}, Ni^{2+}, Cu^{2+}, Zn^{2+}, Pb^{2+}, Cd^{2+}, Ba^+, and Hg^{2+}.

Determination of detection limits

The titration data obtained from the spectroscopic studies were used to set up a calibration curve, Benesi–Hildebrand plot, and calculate the limit of detection (LOD) and the limit of quantification (LOQ) for various chemosensors using eqn (1) and (2):

$$\mathrm{LOD} = 3.3 \times \frac{\sigma}{m} \quad (1)$$

$$\mathrm{LOQ} = 10 \times \frac{\sigma}{m} \quad (2)$$

In the above equations, σ = the standard deviation and m = the slope of the calibration curve.[10,38]

Determination of binding stoichiometry by Job's plot method

The binding ratio between the preferred metal cation and the coumarin-based chemosensor was investigated using Job's plot UV-visible spectroscopic analysis. In this investigation, the molar ratio between the chemosensor and the preferred metal cation varies; however, the total molar concentration remains at 33.33 μM. The molar ratios occur between 0.1 and 1. Job's plot was plotted using the mole fraction *vs.* absorbance. This plot shows the binding ratio between the chemosensor and the preferred metal cation. The point of intersection on the plot determines the binding ratio between the chemosensor and the preferred metal cation.[10,38]

Calculation of the association constant by Benesi–Hildebrand analysis

The binding constant can also be calculated by using the Benesi–Hildebrand plot. The Benesi–Hildebrand plot is then used along with eqn (3):

$$\frac{1}{A_0 - A} = \left(\frac{1}{A_0 - A_{\mathrm{Max}}}\right) + \left(\frac{1}{K[\mathrm{analyte}]n(A_0 - A_{\mathrm{Max}})}\right) \quad (3)$$

In the above equation, A_0 presents the initial absorbance of the chemosensor, A represents the absorbance of the chemosensor in the presence of the analyte, A_{Max} represents the absorbance when the analyte is in excess, [analyte] is the concentration of the metal cation, n is the stoichiometric ratio, and K represents the binding constant. The Benesi–Hildebrand plot was plotted $\frac{1}{(A_0 - A)}$ *vs.* $\frac{1}{[\text{preferred metal cation}]}$.[10,39]

Reversibility studies

The reversibility of the chemosensor complexes was conducted using UV-vis analysis in acetonitrile at room temperature. The study was conducted by adding a single amount of the preferred cation and monitoring the absorbance response of the saturation point. Upon complexation, the hexadentate chelating ligand EDTA was sequentially added to the solution of the complex, and the absorbance response was monitored. No change in the absorbance response indicates no reversibility, and regaining the chemosensor's absorbance spectra indicates complete reversibility.[10]

Computational analysis

Computational analysis of the coumarin-based chemosensor and the complex that forms in the presence of the preferred metal cation was investigated by using Spartan. The conformer distribution was performed at the MMFF level to obtain the different conformers and coordination complexes that can form. The equilibrium geometry was then performed at the density functional level using a ωB97X-D method and a 6-31G* basis set. The molecular modelling calculations were carried

out in the gas phase, and the electron density map was used to visualise the flow of electrons in the complexes that form and determine where the metal cation complexes with the chemosensor. The molecular modelling studies were performed in a vacuum.[10,38]

^{1}H-NMR and ^{13}C-NMR complexation analysis

Titration studies were carried out using ^{1}H-NMR and ^{13}C-NMR spectroscopies to determine the atoms of the chemosensors involved in the complexation with the preferred metal cation. The chemosensor sample was prepared by dissolving a small amount of the sensor in $CDCl_3$. A small aliquot of the preferred metal cation stock solution, dissolved in deionised water, was added to the NMR tube containing the chemosensor. The ^{1}H-NMR and ^{13}C-NMR analyses were run on the chemosensor before the addition of the analyte. After adding the analyte, the spectra were compared to investigate which atoms of the chemosensors were involved in complexation with the selected analyte.[10,38]

Application studies

Colourimetric real-world application studies were performed by spiking water sourced from the North End Lake, Gqeberha, Eastern Cape, South Africa. The water was used to make a 0.05 M solution of Hg^{2+} and Cu^{2+} that was then added to a 3 mL acetonitrile solution containing 10 μL of the chemosensor (0.05 M).

Conclusions

Herein, we successfully synthesised ethyl 2-oxo-2*H*-chromene-3-carboxylate, **S1a**, and ethyl 8-methoxy-2-oxo-2*H*-chromene-3-carboxylate, **S2a**. These compounds were then subjected to thionation using Lawesson's reagent. The reaction resulted in two products: the major product was identified and characterised as the mono-substituted analogues (**S1b** and **S2b**), and the minor product was identified and characterised as the disubstituted analogues (**S1c** and **S2c**) of **S1a** and **S2a**. The substitution of the carbonyl oxygens by sulphur atoms was predicted to occur stepwise in which the carbonyl of the lactone ring was first substituted, followed by a second substitution on the ester moiety. This was supported by following the reaction with TLC plates; the mono-substituted was first synthesised, followed by the appearance of the disubstituted thiocoumarin derivatives.

The mono- and disubstitution effect on **S1a** and **S2a** as a chemosensor for metal ions was investigated in acetonitrile. It was observed that the selectivity changed from Fe^{2+} and Fe^{3+} to Hg^{2+} in the mono-substituted analogues **S1b** and **S2b**. Subsequently, the disubstituted analogues **S1c** and **S2c** were selective for Hg^{2+} and Cu^{2+}. Further studies have shown that **S1a** was not selective for the preferred metal cation, Fe^{3+} and poor selectivity was observed for **S1b** and **S2b** towards Hg^{2+}. However, remarkable selectivity towards Hg^{2+} and Cu^{2+} was observed for **S1c** and **S2c**, with only Fe^{2+} slightly interfering with the selectivity. Furthermore, it was also concluded that **S1c** and **S2c** selected Cu^{2+} above Hg^{2+}.

Lastly, real-world application studies showed that **S2b** could be used as a qualitative colourimetric chemosensor for Hg^{2+}, and **S2c** can be used as both a qualitative and quantitative colourimetric chemosensor for Hg^{2+}. It is recommended that **S2c** is used as a qualitative colourimetric chemosensor for Cu^{2+} due to the high sensitivity towards Cu^{2+}. However, quantitative analysis of the analytes could be performed using a UV-vis spectrophotometer for all sensors tested.

In this paper, we have shown that it is possible to change the selectivity of a chemosensor by substituting the carbonyl oxygens with their sulphur analogues, leading the way to designing chemosensors that are selective for Hg^{2+}.

Author contributions

All authors contributed to the study. The conception and design of this study are credited to Stiaan Schoeman. Stiaan Schoeman and Lisa Myburgh performed compound synthesis, data collection and analysis. Neliswa Mama contributed reagents, analysis tools and funding. The first draft was written by Stiaan Schoeman and subsequently edited by Lisa Myburgh and Neliswa Mama. All authors read and approved the final manuscript.

Data availability

The data supporting this article have been included in the ESI.†

Conflicts of interest

There are no conflicts to declare.

Acknowledgements

The authors acknowledge the financial support from Nelson Mandela University and acknowledge the student bursary support from the National Research Foundation (grant number: 121590 – MND190612447069). The authors also thank and acknowledge Dr Richard Betz (from Nelson Mandela University) for synthesising Lawesson's reagent and Mrs Caryl Janse van Rensburg (from the University of KwaZulu-Natal) for the elemental analysis of thionated compounds.

References

1 K. B. Patel, S. Mukherjee, H. Bhatt, D. Rajani, I. Ahmad, H. Patel and P. Kumari, Synthesis, Docking, and Biological Investigations of New Coumarin-Piperazine Hybrids as Potential Antibacterial and Anticancer Agents, *J. Mol. Struct.*, 2023, **1276**, 134755, DOI: 10.1016/J.MOLSTRUC.2022.134755.
2 S. Zeinali, L. Z. Fekri, M. Nikpassand and R. S. Varma, Greener Syntheses of Coumarin Derivatives Using Magnetic Nanocatalysts: Recent Advances, *Top. Curr. Chem.*, 2023, **381**, 1–71, DOI: 10.1007/S41061-022-00407-4/SCHEMES/11.
3 Y. F. Mustafa, Synthesis, Characterization, and Biomedical Assessment of Novel Bisimidazole–Coumarin Conjugates,

Appl. Nanosci., 2023, **13**, 1907–1918, DOI: 10.1007/S13204-021-01872-X/TABLES/6.

4 X. C. Yang, C. M. Zeng, S. R. Avula, X. M. Peng, R. X. Geng and C. H. Zhou, Novel Coumarin Aminophosphonates as Potential Multitargeting Antibacterial Agents against Staphylococcus Aureus, *Eur. J. Med. Chem.*, 2023, **245**, 114891, DOI: 10.1016/J.EJMECH.2022.114891.

5 L. K. A. M. Leal, A. A. G. Ferreira, G. A. Bezerra, F. J. A. Matos and G. S. B. Viana, Antinociceptive, Anti-Inflammatory and Bronchodilator Activities of Brazilian Medicinal Plants Containing Coumarin: A Comparative Study, *J. Ethnopharmacol.*, 2000, **70**, 151–159, DOI: 10.1016/S0378-8741(99)00165-8.

6 Y. Boulaamane, I. Ahmad, H. Patel, N. Das, M. R. Britel and A. Maurady, Structural Exploration of Selected C6 and C7-Substituted Coumarin Isomers as Selective MAO-B Inhibitors, *J. Biomol. Struct. Dyn.*, 2023, **41**, 2326–2340, DOI: 10.1080/07391102.2022.2033643.

7 C. F. Hu, P. L. Zhang, Y. F. Sui, J. S. Lv, M. F. Ansari, N. Battini, S. Li, C. H. Zhou and R. X. Geng, Ethylenic Conjugated Coumarin Thiazolidinediones as New Efficient Antimicrobial Modulators against Clinical Methicillin-Resistant Staphylococcus Aureus, *Bioorg. Chem.*, 2020, **94**, 103434, DOI: 10.1016/J.BIOORG.2019.103434.

8 S. S. Hamukoshi, N. Mama, J. M. V. Ngororabanga, S. Schoeman, N. H. Shafuda, V. Uahengo and E. Hosten, Synthesis and Characterization of a New Hydrazone-Coumarin Chemosensor for Fe^{3+} in a Water–Acetonitrile Mixture, *ARKIVOC*, 2023, **2023**, 202312030, DOI: 10.24820/ark.5550190.p012.030.

9 S. Hamukoshi, N. Mama, S. Schoeman and V. Uahengo, A Facile Synthesis of a Novel 4-Hydroxyl-3-Azo Coumarin Based Colorimetric Probes for Detecting Hg^{2+} and a Fluorescence Turn-off Response of 3CBD to Fe^{3+} in Aqueous Environment, *RSC Adv.*, 2023, **13**, 31541–31553, DOI: 10.1039/D3RA04047J.

10 A. Battison, S. Schoeman and N. Mama, A Coumarin-Azo Derived Colorimetric Chemosensor for Hg^{2+} Detection in Organic and Aqueous Media and Its Extended Real-World Applications, *J. Fluoresc.*, 2023, **33**, 267–285, DOI: 10.1007/s10895-022-03065-3.

11 C. J. Hua, H. Zheng, K. Zhang, M. Xin, J. R. Gao and Y. J. Li, A Novel Turn off Fluorescent Sensor for Fe(III) and PH Environment Based on Coumarin Derivatives: The Fluorescence Characteristics and Theoretical Study, *Tetrahedron*, 2016, **72**, 8365–8372, DOI: 10.1016/j.tet.2016.08.023.

12 A. D. Johnson, R. M. Curtis and K. J. Wallace, Low Molecular Weight Fluorescent Probes (LMFPs) to Detect the Group 12 Metal Triad, *Chemosensors*, 2019, **7**, 22, DOI: 10.3390/CHEMOSENSORS7020022.

13 T. L. Cottrell, *The Strengths of Chemical Bonds, Properties of atoms, radicals, and bond*, 2nd edn, 1966, vol. 372.

14 S. Croft, Kaye and Laby – Tables of Physical and Chemical Constants (15th Edn), *Phys. Bull.*, 1987, 38, DOI: 10.1088/0031-9112/38/4/037.

15 W. M. Haynes, in *CRC Handbook of Chemistry and Physics*, ed. Haynes, W. M., CRC Press, Boca Raton, 95th edn, 2014, ISBN 9780429170195.

16 J. Nriagu and C. Becker, Volcanic Emissions of Mercury to the Atmosphere: Global and Regional Inventories, In Proceedings of the Science of the Total Environment, 2003, vol. 304.

17 N. Pirrone, S. Cinnirella, X. Feng, R. B. Finkelman, H. R. Friedli, J. Leaner, R. Mason, A. B. Mukherjee, G. B. Stracher and D. G. Streets, *et al.*, Global Mercury Emissions to the Atmosphere from Anthropogenic and Natural Sources, *Atmos. Chem. Phys.*, 2010, 10, DOI: 10.5194/acp-10-5951-2010.

18 D. M. Pyle and T. A. Mather, The Importance of Volcanic Emissions for the Global Atmospheric Mercury Cycle, *Atmos. Environ.*, 2003, **37**(36), 5115–5124, DOI: 10.1016/j.atmosenv.2003.07.011.

19 T. Wajima and K. Sugawara, Adsorption Behaviors of Mercury from Aqueous Solution Using Sulfur-Impregnated Adsorbent Developed from Coal, *Fuel Process. Technol.*, 2011, **92**(7), 1322–1327, DOI: 10.1016/j.fuproc.2011.02.008.

20 B. Ram and G. S. Chauhan, New Spherical Nanocellulose and Thiol-Based Adsorbent for Rapid and Selective Removal of Mercuric Ions, *Chem. Eng. J.*, 2018, **331**, 587–596, DOI: 10.1016/j.cej.2017.08.128.

21 O. Hakami, Y. Zhang and C. J. Banks, Thiol-Functionalised Mesoporous Silica-Coated Magnetite Nanoparticles for High Efficiency Removal and Recovery of Hg from Water, *Water Res.*, 2012, **46**(12), 3913–3922, DOI: 10.1016/j.watres.2012.04.032.

22 V. Polshettiwar and M. Kaushik, Recent Advances in Thionating Reagents for the Synthesis of Organosulfur Compounds, *J. Sulfur Chem.*, 2006, **27**(4), 353–386, DOI: 10.1080/17415990600733112.

23 B. S. Pedersen and S.-O. Lawesson, Studies on Organophosphorus Compounds—XXVIII: Syntheses of 3H-1,2-dithiole-3-thiones and 4H-1,3,2,-oxazaphosphorine derivatives from the dimer of p-methoxyphenyl-thionophosphine sulfide and der, *Tetrahedron*, 1979, **35**(20), 2433–2437, DOI: 10.1016/s0040-4020(01)93760-3.

24 S. A. Patil, S. N. Unki, A. D. Kulkarni, V. H. Naik and P. S. Badami, Synthesis, Characterization, in Vitro Antimicrobial and DNA Cleavage Studies of Co(II), Ni(II) and Cu(II) Complexes with ONOO Donor Coumarin Schiff Bases, *J. Mol. Struct.*, 2011, **985**, 330–338, DOI: 10.1016/J.MOLSTRUC.2010.11.016.

25 I. Ansary and A. Taher, One-Pot Synthesis of Coumarin Derivatives, *Phytochemicals in Human Health*, 2019, ch. 6, DOI: 10.5772/intechopen.89013.

26 W. Du, H. Shi, H. Zhang, J. Zhao, H. Yang and P. Yang, Controlled Asymmetric Aggregation Advances n → Π* Electronic Transition and Charge Separation for Enhanced Photocatalytic Hydrogen Synthesis, *J. Catal.*, 2024, **432**, 115453, DOI: 10.1016/J.JCAT.2024.115453.

27 M. Weller; M. T. Weller; T. Overton; J. Rourke and F. Armstrong, *Inorganic Chemistry*, Oxford University Press, 2014, ISBN 9780199641826.

28 M. Smith and J. March, *Advanced Organic Chemistry: Reactions, Mechanisms, and Structure*, John Wiley & Sons, 8th edn, 2020.

29 R. Kumar Rai, A. Chalana, R. Karri, A. Islam, R. Shankar Pati, V. P. Sarathy and G. Roy, Synthesis, Structures and DFT Study of Copper Coordination with Bis- Benzimidazole

Based Thiones and Selones: Scope for Nonstoichiometric Cu2-XSe Nanoparticles, *Inorg. Chim. Acta*, 2024, **562**, 121880, DOI: 10.1016/J.ICA.2023.121880.

30 V. Pósa, B. Hajdu, G. Tóth, O. Dömötör, C. R. Kowol, B. K. Keppler, G. Spengler, B. Gyurcsik and É. A. Enyedy, The Coordination Modes of (Thio)Semicarbazone Copper(II) Complexes Strongly Modulate the Solution Chemical Properties and Mechanism of Anticancer Activity, *J. Inorg. Biochem.*, 2022, **231**, 111786, DOI: 10.1016/J.JINORGBIO.2022.111786.

31 A. Bonnot, M. Knorr, F. Guyon, M. M. Kubicki, Y. Rousselin, C. Strohmann, D. Fortin and P. D. Harvey, 1,4-Bis(Arylthio)but-2-Enes as Assembling Ligands for $(Cu_2X_2)_n$ (X = I, Br; N = 1, 2) Coordination Polymers: Aryl Substitution, Olefin Configuration, and Halide Effects on the Dimensionality, Cluster Size, and Luminescence Properties, *Cryst. Growth Des.*, 2016, **16**, 774–788, DOI: 10.1021/ACS.CGD.5B01360/SUPPL_FILE/CG5B01360_SI_001.PDF.

32 M. Chaabéne, A. Khatyr, M. Knorr, M. Askri, Y. Rousselin and M. M. Kubicki, Bis{(4-Methylthio)Phenylthio}methane as Assembling Ligand for the Construction of Cu(I) and Hg(II) Coordination Polymers. Crystal Structures and Topological (AIM) Analysis of the Bonding, *Inorg. Chim. Acta*, 2016, **451**, 177–186, DOI: 10.1016/J.ICA.2016.07.023.

33 A. Beheshti, K. Nozarian, E. S. Mousavifard, C. T. Abrahams, P. Mayer, R. Gajda, K. Woźniak and H. Motamedi, Design and Construction of the Imidazole-2-Thione-Based Copper(I) Complexes by Varying the Co-Anion and Synthesis Conditions and Verifying Their Antimicrobial Activity, *J. Solid State Chem.*, 2021, **294**, 121874, DOI: 10.1016/J.JSSC.2020.121874.

34 T.-L. Ho, *Hard and Soft Acids and Bases Principle in Organic Chemistry*, AcademicPress, NewYork, 1977, ISBN 0-12-350050-8.

35 A. E. Laturski, J. R. Gaffen, P. Demay-Drouhard, C. B. Caputo and T. Baumgartner, Probing the Impact of Solvent on the Strength of Lewis Acids *via* Fluorescent Lewis Adducts, *Precis. Chem.*, 2023, **1**, 49–56, DOI: 10.1021/prechem.2c00009.

36 I. Thomsen, K. Clausen, S. Scheibye and S.-O. Lawesson, Thiation with 2,4-Bis(4-methoxyphenyl)-1,3,2,4-dithiadiphosphetane 2,4-disulfide: *N*-methylthiopyrrolidone, *Org. Synth.*, 1984, **62**, 158, DOI: 10.15227/orgsyn.062.0158.

37 H. Khatoon and E. Abdulmalek, A Focused Review of Synthetic Applications of Lawesson's Reagent in Organic Synthesis, *Molecules*, 2021, **26**, 6937, DOI: 10.3390/MOLECULES26226937.

38 N. Mama and A. Battison, Synthesis and Application of a Fluorescent "turn-Off" Triazolyl-Coumarin-Based Fluorescent Chemosensor for the Sensing of Fe^{3+} Ions in Aqueous Solutions, *ARKIVOC*, 2020, **2020**, 59–84, DOI: 10.24820/ARK.5550190.P011.283.

39 F. Fateh, A. Yildirim, A. A. Bhatti and M. Yilmaz, A New Benzothiazin-Functionalized Calix[4]Arene-Based Fluorescent Chemosensor for the Selective Detection of Co^{2+} Ion, *J. Fluoresc.*, 2021, **31**, 1075–1083, DOI: 10.1007/S10895-021-02745-W/TABLES/1.

